Supporting Information

Title: Novel Self-Assembling Approach for Synthesizing Nanofiber Aerogel Supported Platinum Single Atoms

Haojie Zhang,[a,†] Yonghui Zhao,[b,†] Yu Sun,[c] Qing Xu,[b] Ruoou Yang,[d] Hao Zhang,[d] Chao Lin,[a] Kenich Kato,[e] Xiaopeng Li,[a,*] Miho Yamauchi[f,g,*] and Zheng Jiang[d,h,*]

DFT calculation. To see the possible role of atomistic Pt doping in the crystal framework of MnO_2, we exploit the changes in the geometric and electronic effects by Vienna Ab initio Simulation Package (VASP)[S1-3] code based on self-consistent density functional theory (DFT) on the experimentally observed MnO_2(100) surface. Model of Pt doping with atoms substituting Mn sites (denoted Sub-Pt-MnO_2(100)) on the 2×1 MnO_2(100) surface. Throughout all the computations, the spin-polarized calculations were carried out because of the ferromagnetic manner of Mn atoms. The PBEsol (Perdew–Burke–Ernzerhof revised for solids)[S4] parameterization version of the generalized gradient approximation (GGA) was used to incorporate exchange and correlation energies. A DFT plus Hubbard model (DFT +U)[S5] of U_{eff} = 1.6 eV was applied to the Mn d states, which were used in Ref[S6]. In order to avoid the artificial interactions between the surface and its periodic images, a vacuum thickness of 13 Å was added in the slab cell along the direction perpendicular to the surface. For the Brillouin zone integration, a 2 × 4 × 1 Monkhorst−Pack[S7] k-point mesh was used. The self-consistent calculations were repetitively performed until the forces fell below 0.03 eVÅ^{-2} was performed to incorporate surface relaxation effects.

The ORR may proceed through the following elementary steps, and they were considered in the current work:

$$O_2(g) + H^+ + e^- \rightarrow *OOH \quad \text{(S1)}$$

$$*OOH + H^+ + e^- \rightarrow *O + H_2O \quad \text{(S2)}$$

$$*O + H^+ + e^- \rightarrow *OH \quad \text{(S3)}$$

$$*OH + H^+ + e^- \rightarrow H_2O \quad \text{(S4)}$$

where (g) and * represents the gaseous phase and adsorption state, respectively. The adsorption free energy for each species (X = O*, OH*, OOH* and H*) was calculated according to the formula:

$$G_X = E_X + E_{ZPE} - TS \quad \text{(S5)}$$

where E_X is the DFT calculated total energy, E_{ZPE} is the zero-point energy. All the adsorption free energy G_X (X = O*, OH*, OOH* and H*) are relative to the free energy of stoichiometrically

appropriate amounts of H_2O (g) and H_2(g). Given that the high-spin ground state of the oxygen molecule is poorly described in DFT calculations, the free energy of the O_2 molecule was derived according to $G_{O2}(g) = 2G_{H2O}(g) - 2G_{H2}(g) + 4 \times 1.23$ (eV). For each elementary step, the Gibbs reaction free energy ΔG is calculated according to the formula:

$$\Delta G = \Delta E + \Delta ZPE - T\Delta S \quad \text{(S5)}$$

where ΔE is the reaction energy of reactant and product molecules adsorbed on the catalyst surface, obtained from DFT calculations; ΔZPE and ΔS are the change in zero-point energies and entropy due to the reaction. Computational hydrogen electrode (CHE) method was used to calculate the free energy changes of the above elementary steps.[S8]

ORR catalytic measurements. The ORR catalytic measurements were carried out on the Rotating Disk Electrode (RDE, Pine, USA) with the polished glass carbon (Pine, 5 mm diameter, 0.196 cm^2) as the working electrode. The preparation method of the working electrodes containing investigated catalysts can be found as follows. In short, 2 mg of catalyst powder was dispersed in 1/1 (v/v) of water and ethanol mixed solvent with 120 μL of Nafion solution (5 wt%, Sigma-Aldrich), then the mixture was ultrasonicated for 30 min to generate a homogeneous ink. Next, 7.5 μL of dispersion was transferred onto the glassy carbon disk, leading ~ 0.68 μg/cm^2. Finally, the as-prepared catalyst film was dried at room temperature.

Before the electrochemical measurement, the 1 M KOH electrolyte was bubbled O_2 for at least 30 min. The polarization curves were obtained by sweeping the potential from 1.1 to 0.2 V (vs. RHE) at room temperature at 225, 400, 625, 900, 1025 and 1600 rpm, with a sweep rate of 10 mV/s. The electrochemical impedance spectrum was collected at the 0.8 V (vs. RHE).

The transferred electron numbers per O_2 involved in the oxygen reduced were determined by the Koutechy-Levich equation was given below:[S9]

$$\frac{1}{j} = \frac{1}{j_k} + \frac{1}{B\omega^{0.5}} \quad \text{(S7)}$$

Where j is the measured current density, j_k is the kinetic current of the ORR and ω is the angular velocity, $\frac{1}{B}$ is the slope of the *K-L* plots.

$$B = 0.62nF(D_O)^{2/3}v^{-1/6}C_O \quad \text{(S8)}$$

Where n represents number of electrons transferred per oxygen molecule, F is the Faraday constant (F = 96500 C mol^{-1}), D_O is the diffusion coefficient of O_2 in the electrolyte (1.9×10^{-5} cm^2 s^{-1}), v is the kinetic viscosity (0.01 cm^2 s^{-1}), and C_O is the bulk concentration of O_2 (1.2×10^{-6} mol cm^{-3}). The constant 0.2 is adopted when the rotation speed is expressed in rpm.

The transferred electron number (n) and peroxide yield (%H_2O_2) were also measured by the Rotating Ring Disk Electrode (RRDE, Pine, USA) with a polished E7R9 glass carbon as working electrode (Pine, collect efficiency 37%). The recipe of the sample ink and catalyst loading was kept consistent with that of the RDE measurement. The corresponding transferred electron number and peroxide yield was calculated by the equations as bellow:[S10]

$$n = \frac{4I_d}{I_d + I_r/N} \quad \text{(S9)}$$

$$\%H_2O_2 = \frac{4I_r/N}{I_d + I_r/N} \times 100\% \quad \text{(S10)}$$

Where I_d and I_r were the current density of the disk and ring of the RRDE, respectively. N is the RRDE collection efficiency, which was determined to be 0.37 herein.

The kinetic current density was calibrated as bellow,[S9, 11]

$$j_k = \frac{j_d - j}{j_d \times j} \quad \text{(S11)}$$

Where the j_d and j are the diffusion-limited current density and experimentally measured current density, respectively. j_k is the calculated kinetic current density. To better understand the catalytic mechanism, the kinetic current density was normalized to the loading amount of the Pt in the prepared samples to obtain the mass activities.

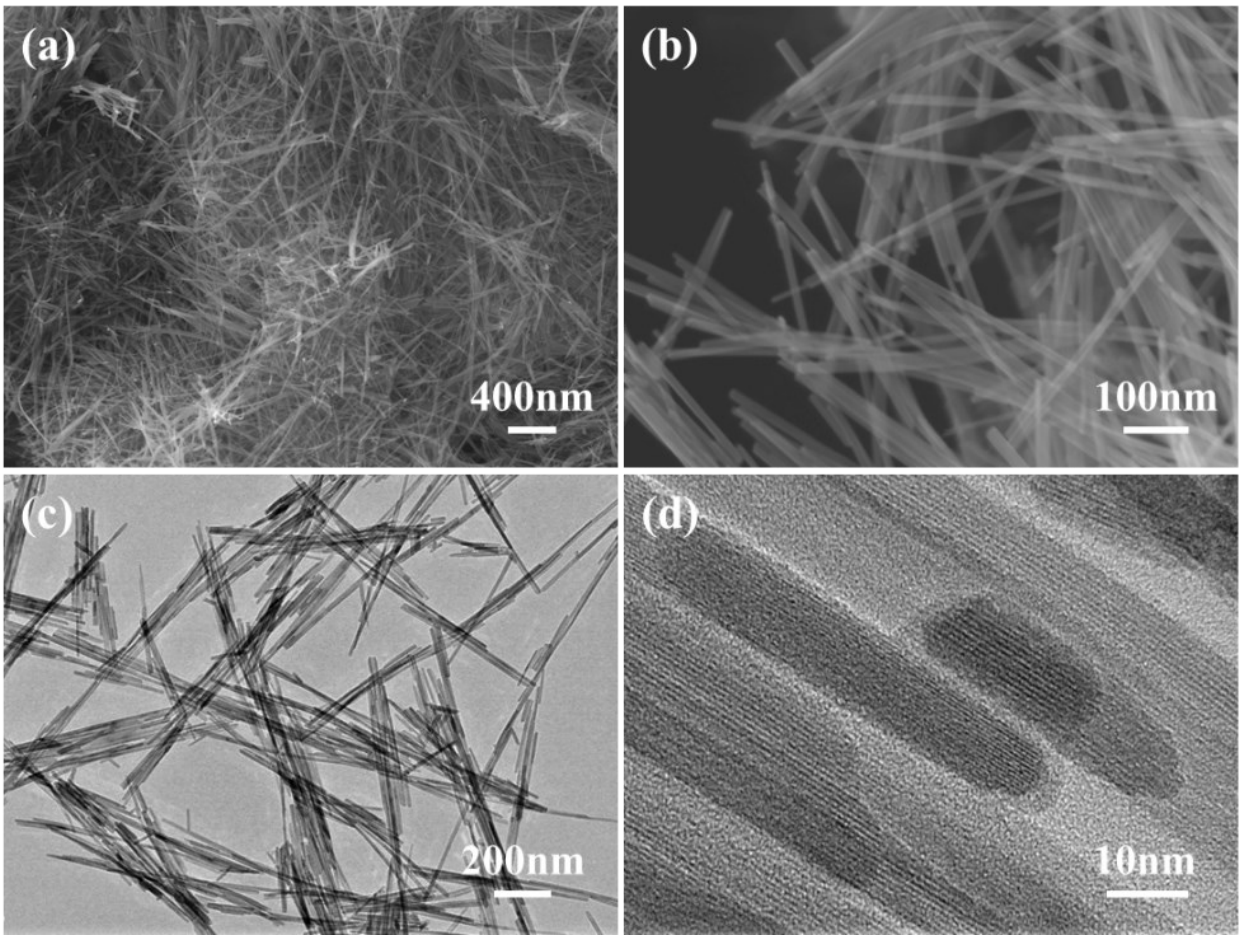

Fig. S1. (a, b) SEM and (c, d) TEM images of un-doped α-MnO_2 nanofibers.

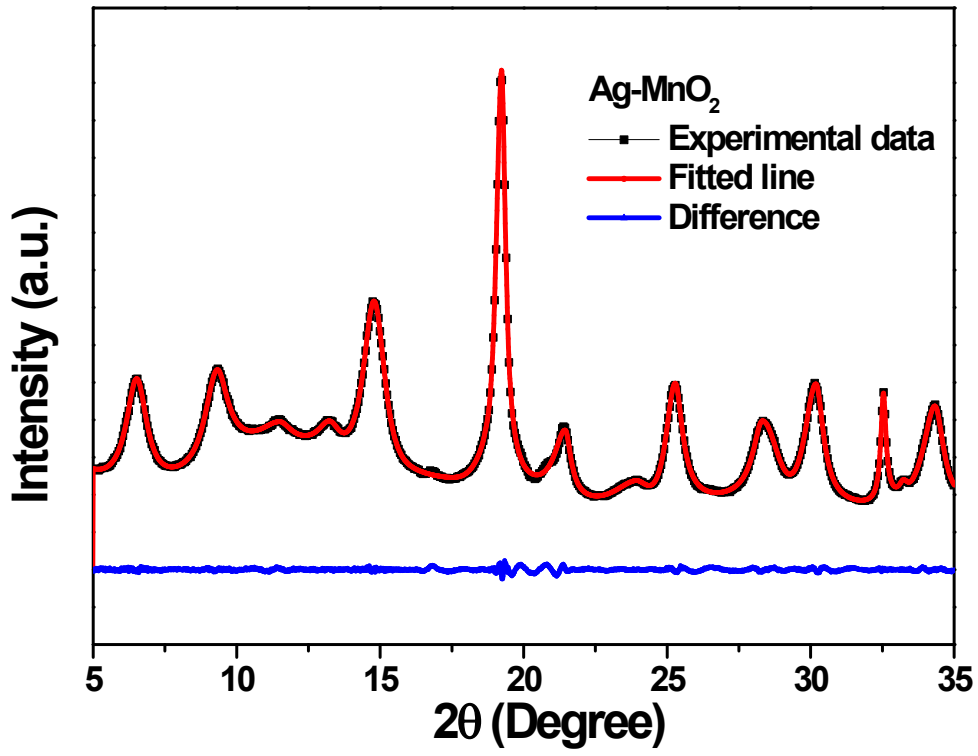

Fig. S2. SRXRD patterns of the Ag/MnO_2.

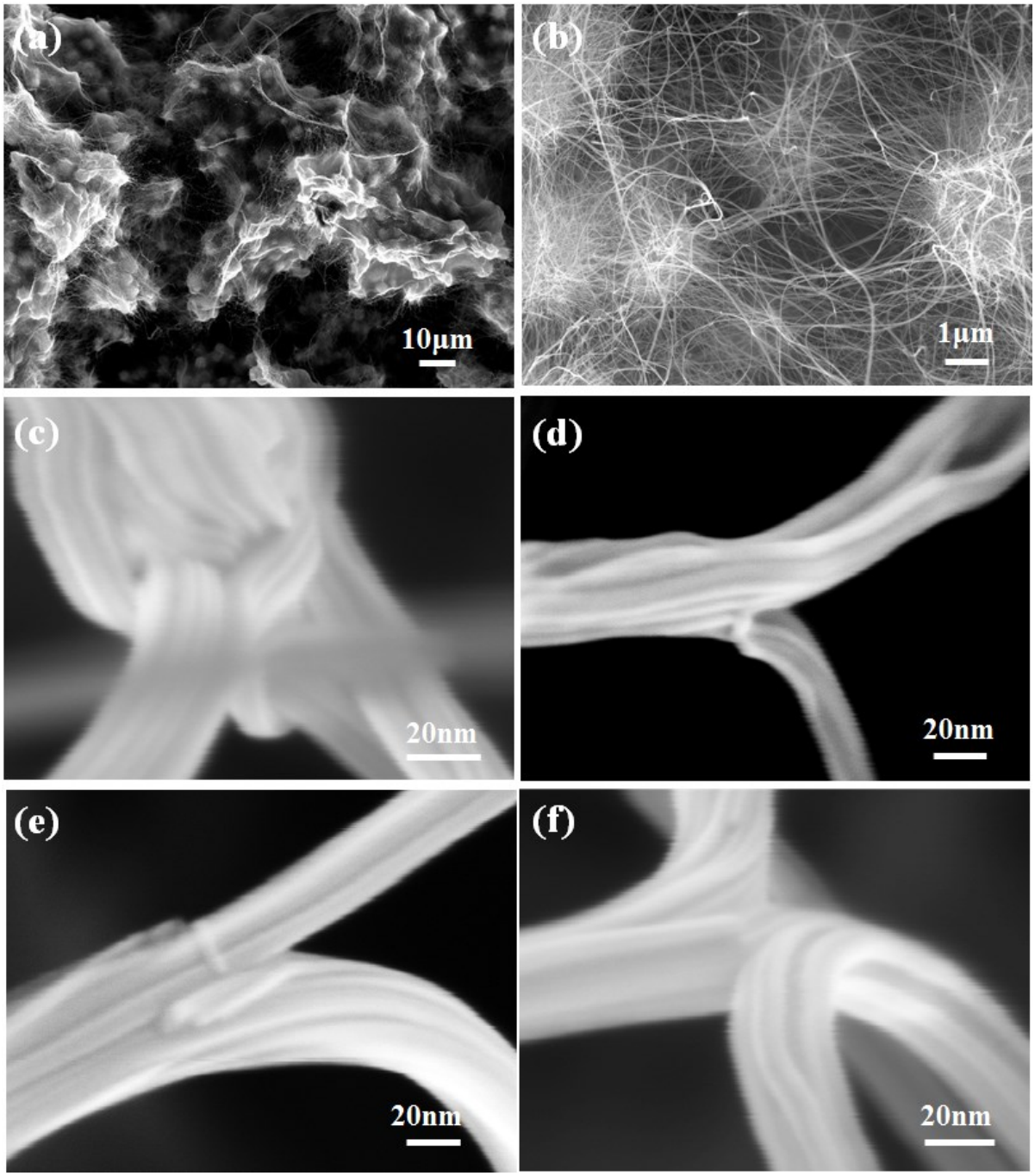

Fig. S3. (a, b) SEM images of Ag-MnO_2 aerogel at different magnifications. (c-f) show various bonding patterns between the Ag-MnO_2 nanofibers.

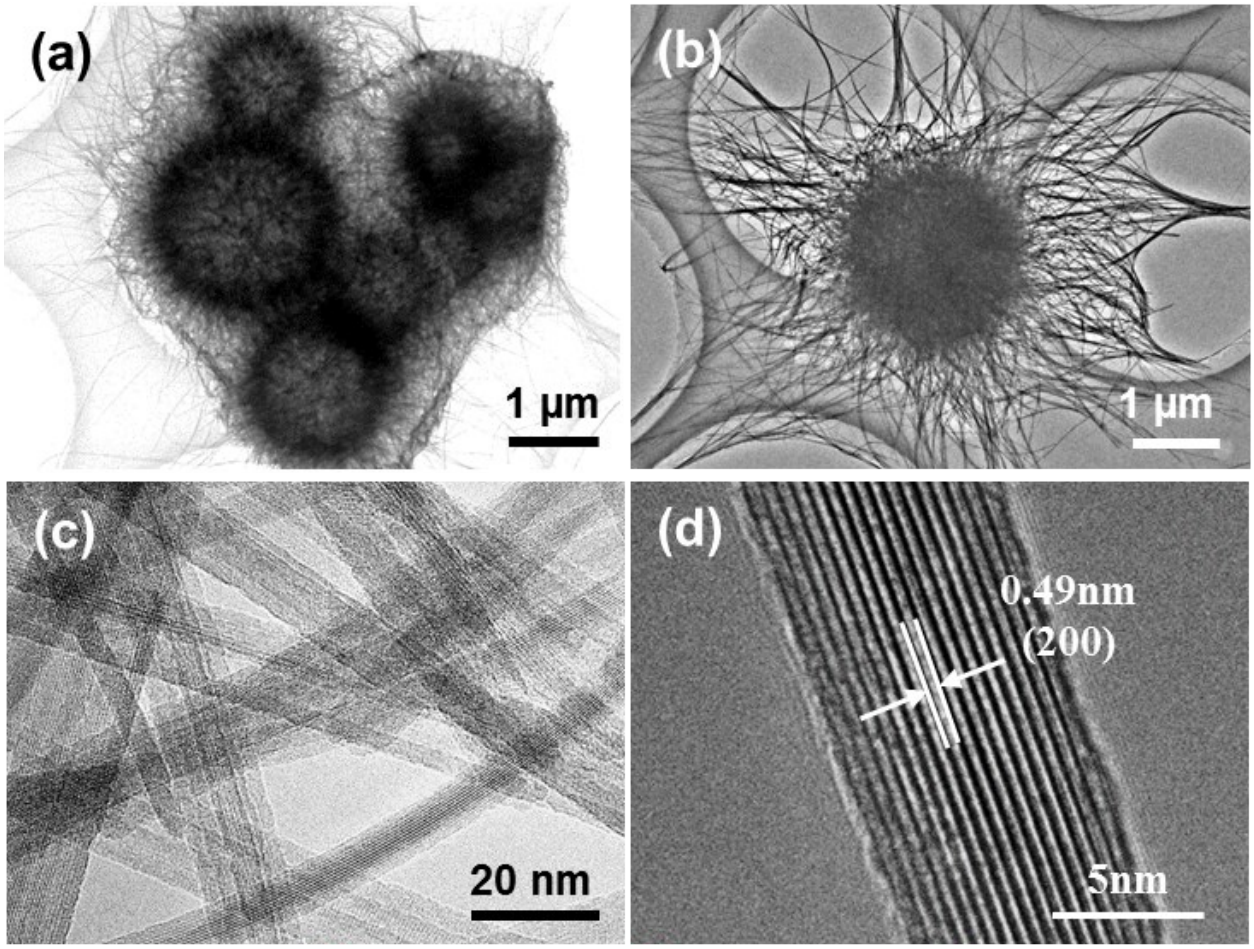

Fig. S4. (a, b) TEM images of the spherical cellular structure in Ag-MnO_2 aerogel. (c, d) high-resolution TEM images of the as-prepared MnO_2 nanofibers.

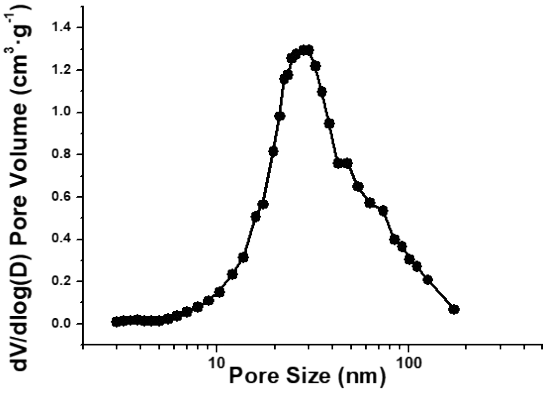

Fig. S5. The pore size distribution of Ag-MnO_2 aerogel.

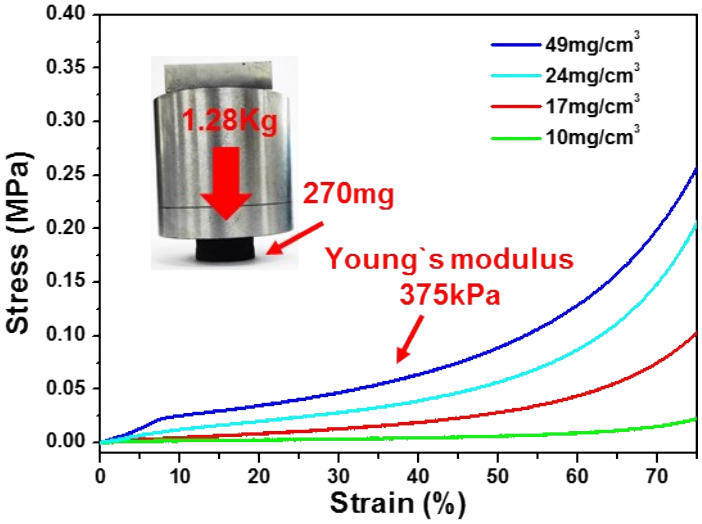

Fig. S6. Compress test of the aerogel along with the different density. The inset picture shows the as prepared aerogel bears ×4740 weight than its own weight without obvious collapse.

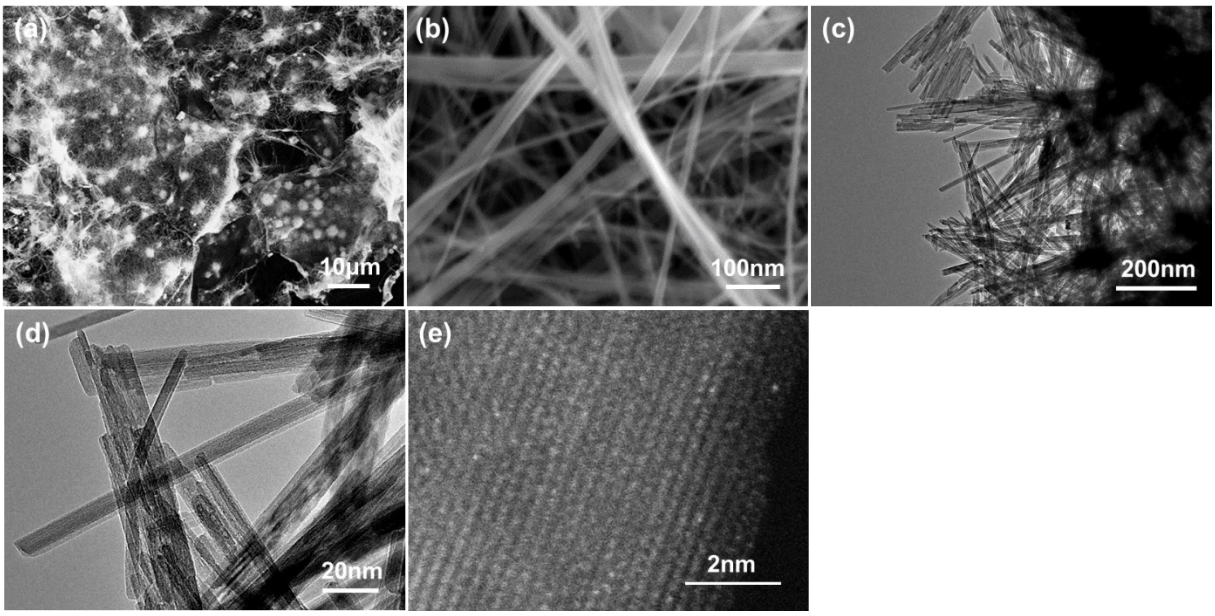

Fig. S7. (a, b) SEM images and (c, d) TEM images of the Pt/Ag-MnO_2 aerogel. (e) HAADF-STEM image of the Pt/Ag-MnO_2 nanofiber.

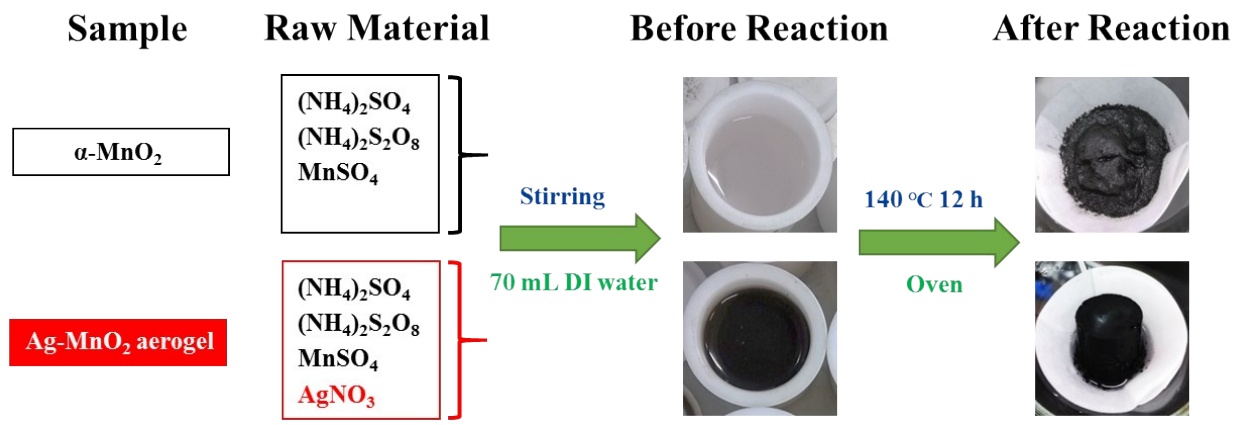

Fig. S8. Schematic process of preparation of un-doped α-MnO_2 nanowire powder and Ag-MnO_2 aerogel.

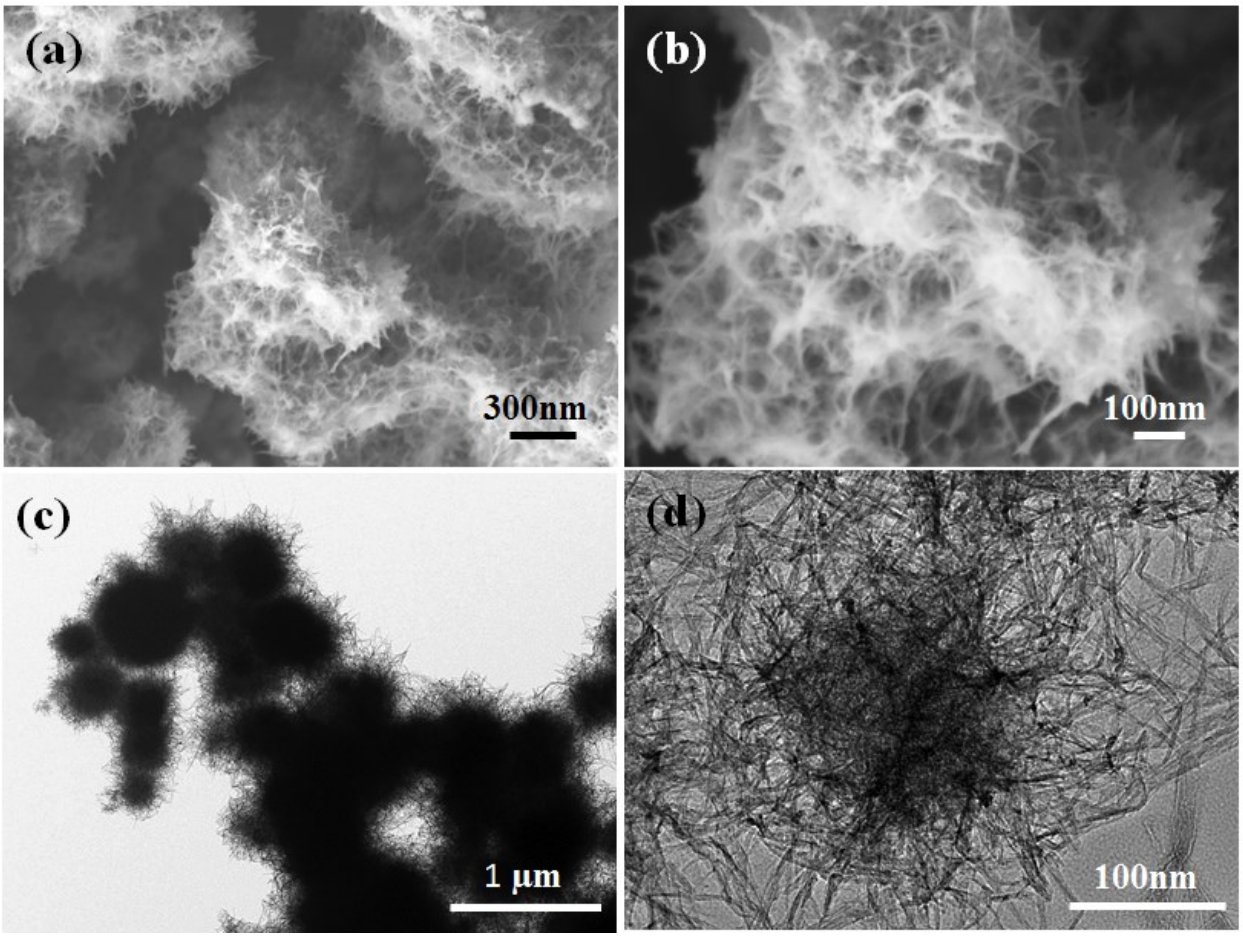

Fig. S9 (a, b) SEM and (c, d) TEM images of the black Ag-MnO_2 nanofiber precipitates formed prior to hydrothermal reaction.

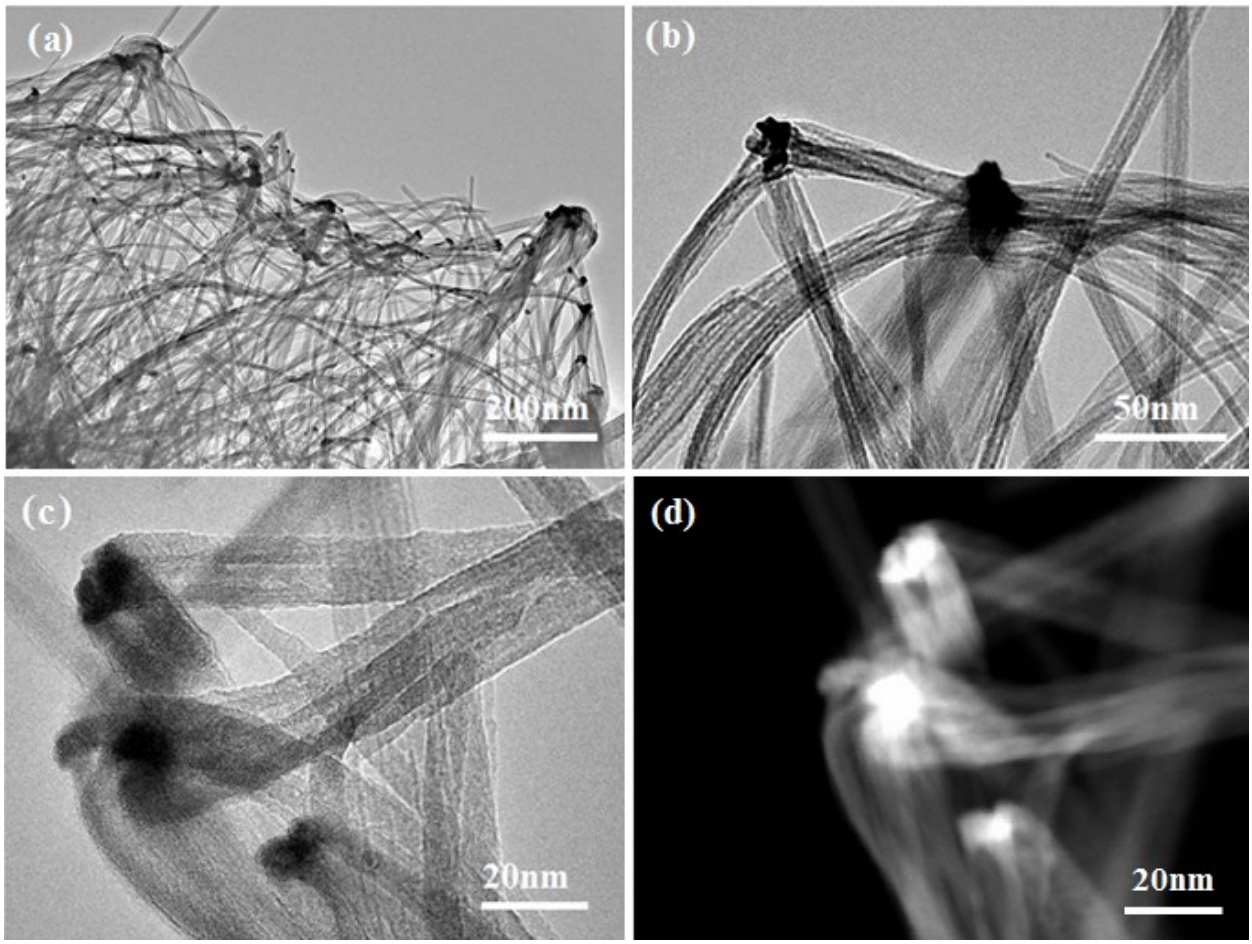

Fig. S10. (a-c) TEM and (d) HAADF-STEM images of the Ag-MnO_2 aerogel formed at the hydrothermal reaction time of 6 h.

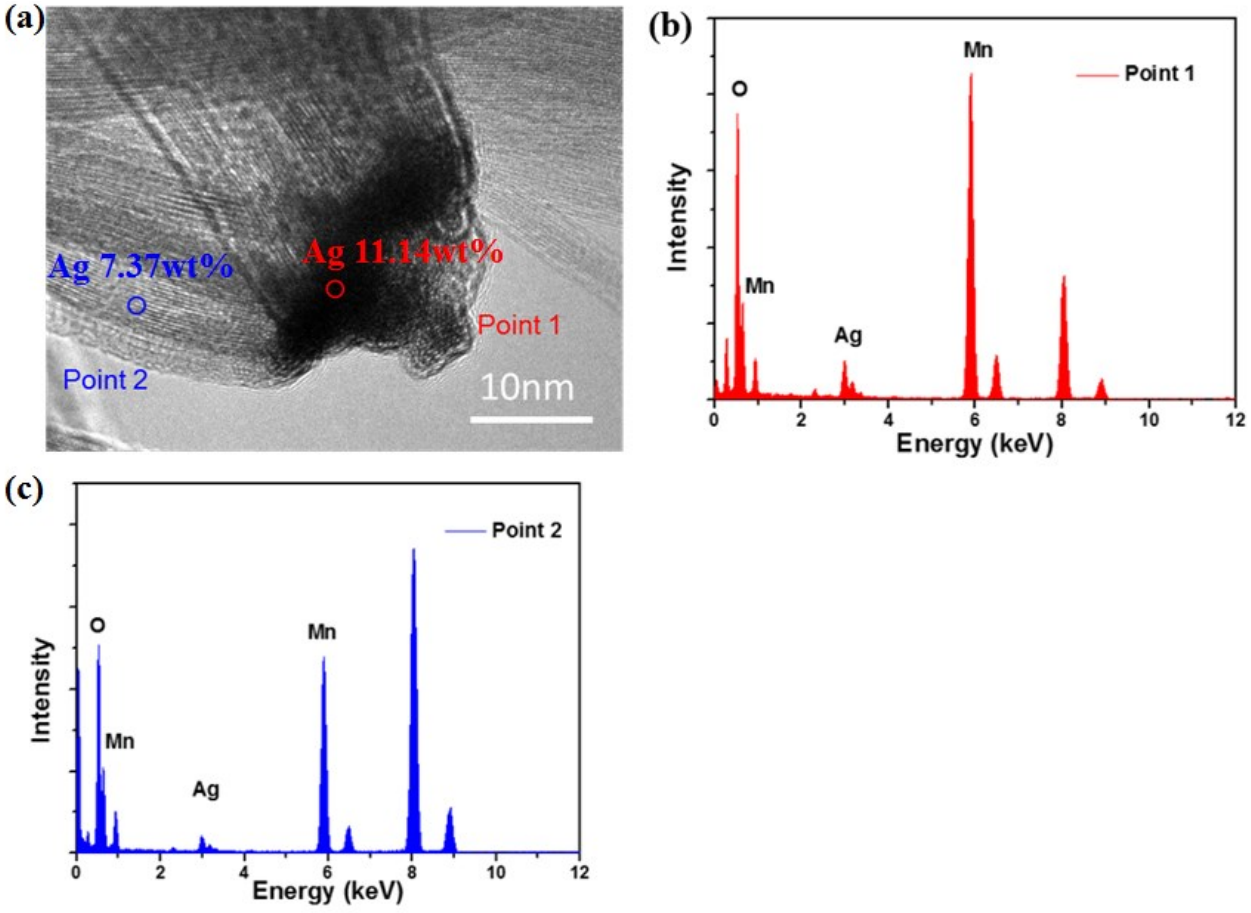

Fig. S11. (a) TEM view of reaction intermediates of the Ag-MnO_2 aerogel formed at the hydrothermal reaction time of 6 h. (b, c) EDS of the point 1 and point 2 in (a).

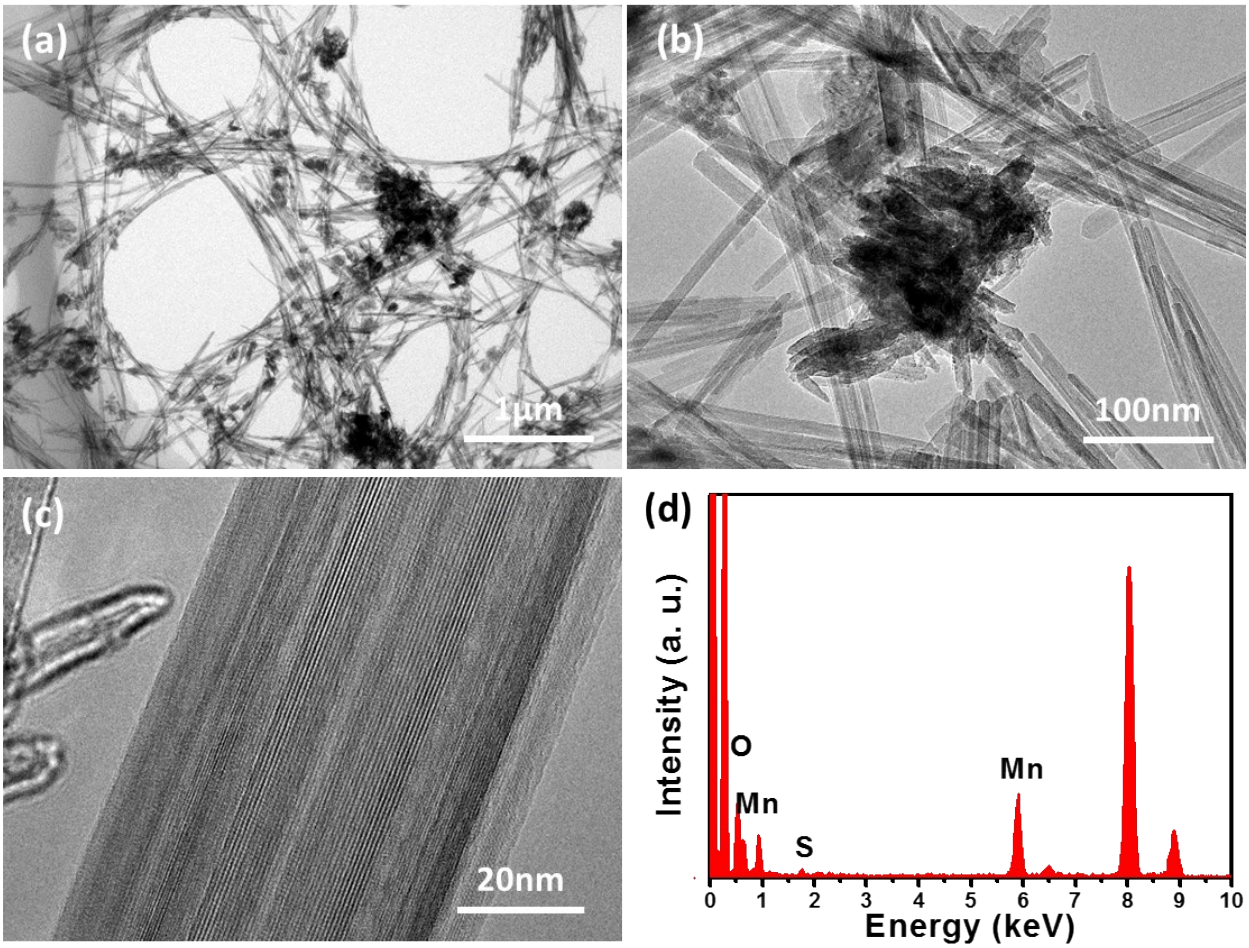

Fig. S12. (a-c) TEM images of the as-prepared Pt-MnO_2 without $AgNO_3$. (d) The corresponding EDS spectra of the signal nanofiber shown in (c).

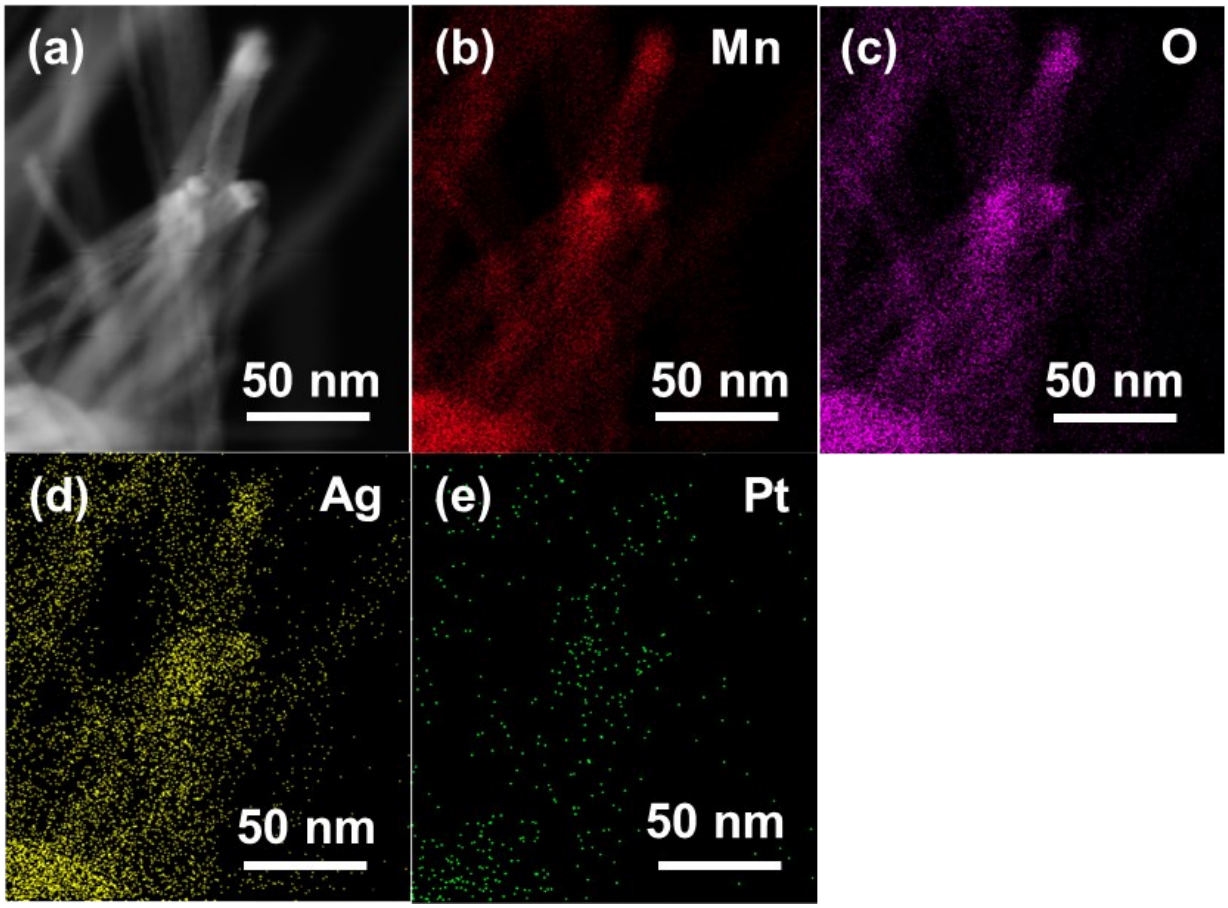

Fig. S13. EDS mapping of the intermediates during the growth of the Pt/Ag-MnO_2 nanofibers. (a) TEM image (b-c) the corresponding EDS mapping images of the Mn, O, Ag and Pt.

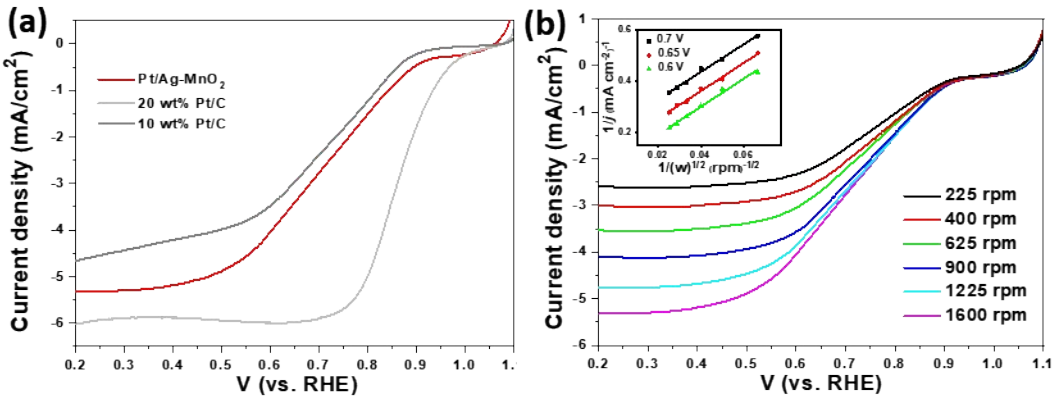

Fig. S14. (a) ORR polarization curves of Pt/Ag-MnO_2, 20 wt% Pt/C and 10 wt% Pt/C. (b) Rotating disk electrode voltammograms of Pt/Ag-MnO_2 at various rotational speeds: 225, 400, 625, 900, 1225 and 1600 rpm. The K-L plot was shown in the inset image.

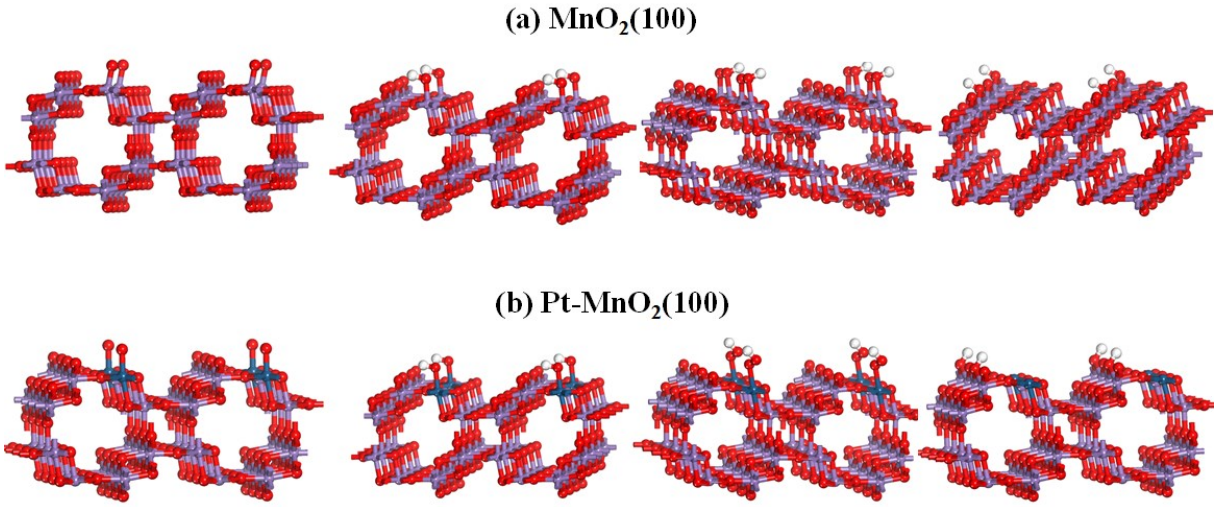

Fig. S15. Adsorption configurations of different ORR intermediates (O*, OH*, OOH*, H) on (a) MnO_2(100) (b) Pt-MnO_2(100). The purple, blue red and white balls represent Mn, Pt, O and H atoms, respectively.

Reference:

S1. G. Kresse and J. Furthmuller, *Comput. Mater. Sci.*, 1996, **6**, 15-50.

S2. G. Kresse and J. Furthmüller, *Phys. Rev. B*, 1996, **54**, 11169-11186.

S3. G. Kresse and J. Hafner, *Phys. Rev. B*, 1993, **47**, 558.

S4. J. P. Perdew, A. Ruzsinszky, G. I. Csonka, O. A. Vydrov, G. E. Scuseria, L. A. Constantin, X. Zhou and K. Burke, *Phys. Rev. Lett.*, 2008, **100**, 136406.

S5. V. I. Anisimov, J. Zaanen and O. K. Andersen, *Phys. Rev. B*, 1991, **44**, 943-954.

S6. E. Cockayne and L. Li, *Chem. Phys. Lett*, 2012, **544**, 53-58.

S7. H. J. Monkhorst and J. D. Pack, *Phys. Rev. B*, 1976, **13**, 5188.

S8. J. K. Nørskov, J. Rossmeisl, A. Logadottir, L. Lindqvist, J. R. Kitchin, T. Bligaard and H. Jónsson, *The Journal of Physical Chemistry B*, 2004, **108**, 17886-17892.

S9. C. Lin, S. S. Shinde, Z. Jiang, X. Song, Y. Sun, L. Guo, H. Zhang, J.-Y. Jung, X. Li and J.-H. Lee, *J. Mater. Chem. A*, 2017, **5**, 13994-14002.

S10. J. Zhang, Z. Xia and L. Dai, *Science Advances*, 2015, **1**, e1500564.

S11. B. Lim, M. Jiang, P. H. Camargo, E. C. Cho, J. Tao, X. Lu, Y. Zhu and Y. Xia, *Science*, 2009, **324**, 1302-1305.